

## OVERVIEW

This paper presents the theoretical basis of the single-source cooling tower model that forms the basis for single and multiple tower predictive results in the SACTI system. It includes a discussion of both calibration and validation of the model.

It was published in *Atmospheric Environment*, **Vol. 25A**, No. 8, pp. 1559-1576, 1991.

This file was scanned from a somewhat water-damaged reprint of the article. If you need better quality, please photocopy the paper from the journal itself.

## A SECOND-GENERATION MODEL FOR COOLING TOWER PLUME RISE AND DISPERSION—I. SINGLE SOURCES

R. A. CARHART

Physics Department, University of Illinois at Chicago, Box 4348, Chicago, IL 60680, U.S.A.

and

A. J. POLICASTRO

Environmental Assessment and Information Sciences Division, Argonne National Laboratory, Argonne,  
 IL 60439, U.S.A.

(First received 9 April 1990 and in final form 29 October 1990)

**Abstract**—A second-generation verified integral model for single-source cooling tower plume dispersion is presented. The formulation of the model contains more physics than other contemporary integral models. Its predictions are compared with 59 field data cases and with 47 laboratory data cases, as well as with the predictions of several other models known to yield relatively accurate results. For single-source data, the model performs as well as the two most accurate integral models from the group of 14 we have tested. However, unlike those other two models, the model developed by Argonne National Laboratory and the University of Illinois (the ANL/UI model) is formulated to predict plumes from multiple sources also. For field data, the model is able to predict visible plume rise within a factor of 2.0 in 75% of cases, and visible plume length within a factor of 2.5 in 70% of cases. For laboratory data, the mean error in trajectory predictions is 20% of rise, and the mean error in dilution predictions is 30%. For one-dimensional integral models these are now state-of-the-art levels of predictive accuracy.

**Key word index:** Plume model, cooling tower, atmospheric diffusion, numerical modeling, integral model, environmental impacts of electrical generation.

### NOMENCLATURE

Units are all in the meter-kilogram-second system with temperatures in Kelvin, except as noted. The number of the equation, section or table where the symbol is first used is given in parentheses after the definition:

a, p	As subscripts, 'ambient' and 'plume' (1, 3)	$N_2$	number of $\rho_j$ values between 0.5 and 2.0 (29)
$C_L$	ratio of wake cavity length to plate characteristic length (24)	$N_{2.5}$	number of $\rho_j$ values (length only) between 0.4 and 2.5 (30)
$C_3$	coefficient for entrainment due to atmospheric diffusion (25)	$N_5$	number of $\rho_j$ values between 0.2 and 5.0 (31)
$C_H$	length parameter for cavity height above tower (17)	$N_F$	number of data cases where no definite prediction was made (32)
$C_L$	length parameter for cavity extent downwind of plate (17)	0	as subscript refers to values at tower exit plane (17)
$C_p$	specific heat at constant pressure of dry air ( $J kg^{-1} °C^{-1}$ ) (6)	$P_H$	one-half of equivalent plate height (19)
$C_w$	length parameter for cavity width from centerline (17)	$P_w$	equivalent plate width (19)
$C_{wf}$	calibration constant for vertical force due to wake section (17)	$Q_s$	saturation mixing ratio at temperature $T$ , pressure $p$ (section 3.8)
$C_e$	ratio of wake entrainment velocity to rms turbulence velocity (23)	$R_a$	plate aspect ratio (18)
$D$	NDCT outlet diameter ( $= 2R_0$ ) (section 5.2)	$r_b$	effective radius of equivalent plate wake (21)
$F_0$	initial densimetric Froude number	$R_m$	radius of 'momentum' plume (1)
$g$	acceleration of gravity ( $9.806 m s^{-2}$ ) (11)	$R_0$	NDCT outlet radius (section 3.5)
$h$	height of NDCT (Table 2)	$R_w$	radius of 'moisture' plume (section 3.1)
$H$	height of tower housing (1/2 of effective plate height) (section 3.7)	$R$	radius of 'temperature' plume (section 3.1)
$k$	crossflow ratio: wind speed at tower top/(exit velocity) (section 4.1)	$s$	distance along plume centerline (Fig. 1)
$L_v$	latent heat of evaporation of water ( $J kg^{-1}$ ) (6)	$T_{a,p}$	temperature of ambient, plume (Kelvin) (6, 11)
		$U$	ambient air velocity, function of $z$ ( $m s^{-1}$ ) (9)
		$V_x$	plume horizontal velocity, function of $s$ ( $m s^{-1}$ ) (4)
		$V$	total plume velocity: $(W^2 + V_x^2)^{1/2}$ (1)
		$V_e$	normal bent-over plume entrainment velocity (3)
		$V'_e$	alternate entrainment velocity due to wake turbulent mixing (23)
		$V''_e$	alternate entrainment velocity in atmospheric diffusion phase (25)
		$W$	plume vertical velocity, function of $s$ ( $m s^{-1}$ ) (5)
		$X_{a,p}$	mixing ratio of water vapor in ambient, plume (g/gda) (14, 7)
		$X_C$	downwind extent or length of wake cavity (24)
		$x$	downwind distance from center of tower exit (Fig. 1)

$z$	distance above tower exit (Fig. 1)
$l$	plate characteristic length (18, 20)
*	as superscript denotes virtual temperatures (11)
$\Delta$	shape function for turbulence intensity in wake (18, 22)
$\Delta x_p$	upwind offset of plate from tower geometrical center (Table 2)
$\Pi$	defined as: $-\rho_a g (\partial Q_s / \partial p)$ (14)
$\Phi_{l/w}$	plume liquid water flux (8)
$\Phi_e$	plume enthalpy flux (6)
$\Phi_{hm}$	plume horizontal momentum flux (4)
$\Phi_m$	plume mass flux (1)
$\Phi_{tw}$	plume total water flux (7)
$\Phi_{vm}$	plume vertical momentum flux (5)
$\alpha$	first entrainment coefficient (1)
$\beta$	second entrainment coefficient (1)
$\gamma_d$	dry adiabatic lapse rate ( $\approx 0.01 \text{ }^\circ\text{C m}^{-1}$ ) (12)
$\theta$	angle of plume centerline with respect to the horizontal (9)
$\lambda$	ratio: (area of moisture core)/(area of temperature plume) (6)
$\mu$	fractional entrainment rate defined in Equation (3)
$\nu$	ratio: (area of momentum plume)/(area of temperature plume) (11)
$\rho_a$	ambient air density ( $\text{kg m}^{-3}$ ) (3)
$\rho_j$	ratio: (predicted value)/(observed value) for $j$ th data point (29)
$\rho_p$	density of plume air, pointwise (12)
$\bar{\rho}_p$	density of plume air averaged over momentum radius (1)
$\bar{\rho}_{log}$	absolute-log-mean of predicted/observed ratios (34)
$\bar{\rho}_j$	mean of predicted/observed ratios (33)
$\sigma_u$	rms longitudinal turbulence velocity in the wake of the tower (18)
$\sigma$	liquid water mixing ratio (gm/gmda) (6)
$\sigma_m$	standard deviation of $\rho_j$ distribution (Table 4)
$\sigma_{log}$	standard deviation of distribution of $ \log_{10} \rho_j $ values (Table 4)
$\tau$	defined as: $\partial Q_s / \partial T$ (14)
$\chi$	defined as: $\lambda L_v \tau / C_p$ (14)

## 1. INTRODUCTION

Numerous mathematical models are available in the literature for predicting the dispersion of vapor plumes from natural draft cooling towers (NDCTs) and from mechanical draft cooling towers (MDCTs). The successes and failures of over a dozen of these competing models have been presented in an extensive study by Carhart *et al.* (1982). In that paper, the performance of each model was compared with field data from five studies and laboratory data from one investigation. In addition, the theoretical formulations of the models were analysed to determine the causes of the model/data discrepancies observed. The study concluded that the existing models needed improvement in five areas.

(1) The models could not simultaneously predict correct bending and dilution. Models that predicted correct bending significantly overpredicted dilution. Models that predicted correct dilution led to too little bending.

(2) The feedback effects on plume dynamics resulting from the treatment of thermodynamics (condensation and evaporation) in these models were too great.

(3) The models contained an inadequate treatment or no treatment of the effects of tower wake on plume trajectory and dilution.

(4) Most models had no treatment or an incorrect treatment of atmospheric diffusion effects. Once the effects of initial momentum and buoyancy die out, atmospheric diffusion is very important for long plumes.

(5) The treatment of plume merging for multiple sources is oversimplified, leading to poor predictions of plume size and location from multiple sources.

Except for item 5, all of these problems have been addressed by improvements embodied in the ANL/UI model for single source cooling tower plume dispersion presented in this paper. Item 5 has been treated in the multiple-source-plume extension of the model, which will be detailed in Part II of this paper.

A major reason for the generally poor performance of existing models based on the large plume data base presented in Carhart *et al.* (1982) is that most of these models were developed at a time when good cooling-tower plume data were unavailable. Over the past several years, however, excellent data have been acquired, and these data permit the development of second-generation models that: (a) avoid the theoretical problems attendant with the first-generation models, as enumerated above, and (b) compare well with the newly acquired laboratory and field data.

The purpose of this paper is to present a model that provides new theoretical solutions to problem areas 1-4 above and that also performs well in tests with the new data base. This data base includes laboratory data from the U.S. and France, and field data from single-source cooling towers at Chalk Point, MD, and Paradise, KY, in the U.S., at Lünen and Philippsburg in the F.R.G., and at Gardanne in France.

## 2. CURRENT STATUS OF SINGLE-SOURCE COOLING TOWER PLUME MODELS

The practical requirements of a cooling-tower plume model are that it should: (a) be inexpensive to run (to allow a large number of cases to be simulated), and (b) provide good single-case accuracy. Two basic types of single-source model have been developed to try to meet these two requirements: closed form and integral. In the closed-form models, algebraic equations are obtained for plume trajectory and plume properties as a function of distance along the centerline, or distance downwind. While such models are the least expensive to run, they sacrifice accuracy of plume representation under the full range of ambient

conditions. By contrast, in the integral models, a set of coupled ordinary non-linear differential equations are solved to yield plume trajectory and properties. Although the integral models are obviously more expensive to run, they offer better predictive accuracy, especially in cases where plume predictions are very sensitive to details of the ambient profiles. The closed-form models are basically integral models with additional simplifying assumptions that allow closed-form integration of the equations.

Because the ANL/UI model is of the integral type, only existing integral model formulations will be considered for comparison. Integral models conserve fluxes of physical plume properties, while representing the progressive dilution of the plume by mixing with a progressively larger volume of ambient air. All models contain an entrainment assumption to represent this mixing of the original plume air with ambient air, usually by specifying a parameterized entrainment velocity. The rate at which ambient air is being incorporated into the plume is obtained by multiplying this velocity by the circumference of the plume and the thickness of the differential slice, as in Fig. 1. The differential equations of the model are represented by the conservation of mass, horizontal momentum, vertical momentum, enthalpy, and total water (with the assumption of 100% relative humidity (r.h.) when liquid water is present).

To formulate the improved, ANL/UI, model a 'generic model' was used, in which a number of competing assumptions gleaned from the other integral models in our earlier Carhart *et al.* (1982) study were included in the model code and were integer-switch selected. This procedure allowed investigation of a wider range of possible assumptions for each significant aspect of model formulation. Included were three entrainment assumptions; several drag force formulas; different spreading rates for heat, moisture; and momentum; and the use or omission of

energetic effects of moisture thermodynamics. For calibration purposes, a large data base was used to identify a clearly superior set of physically plausible assumptions. When examined theoretically, these assumptions also seemed to agree best with what is known about plume structure and behavior.

The most important factor in accurately predicting plume evolution is the mass entrainment rate, which governs the rate of dilution of plume properties. Several popular entrainment assumptions were compared in the generic model. All models assume an Archimedes-type buoyancy force acting on the plume to increase its vertical velocity. On the other hand, the entrained air brings with it zero vertical momentum, thus tending to reduce the plume's vertical velocity. The horizontal momentum brought into the plume with the entrained air causes the plume's horizontal velocity to increase. If no additional forces act on the plume, the relationship between the dilution rate of the plume and its rate of bendover is thus determined.

Some models assume no additional real or effective forces. These models either predict plumes that bend over too slowly, or have a visible region that is too short, showing overdilution. To resolve these problems in the ANL/UI model, the 'bentover plume' assumption (an effective force) is employed, and vertical forces from the tower wake region are also included. The bentover plume assumption requires that at tower exit, horizontal plume velocity equals ambient wind speed. Furthermore, experimental data suggest that the plume has an internal structure with a smaller 'heat core' and a larger 'momentum core' in the plume cross-section (see George *et al.*, 1976; Briggs, 1975; Nakagome and Hishida, 1977). In light of these data, the ANL/UI model utilizes two different radii: one for the temperature-elevated region, and a larger one for the region where plume velocity differs from the ambient, as illustrated in Fig. 2. The physical effect of assuming two radii is that the smaller heated

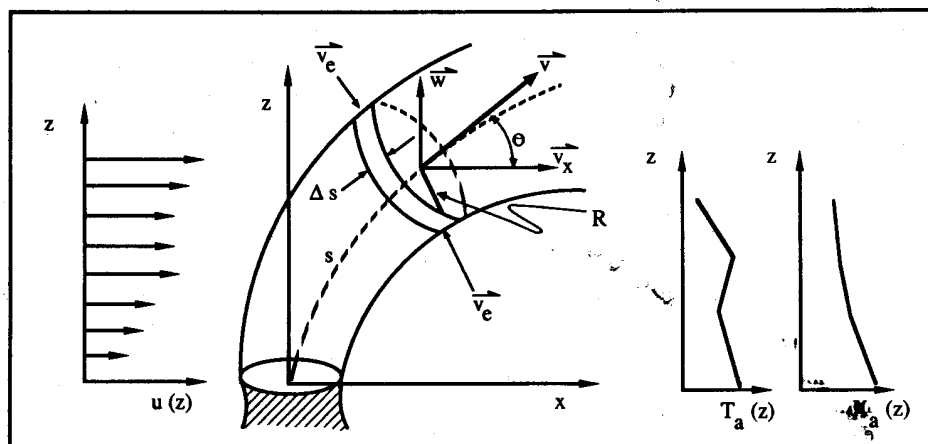


Fig. 1. Quantities representing ANL/UI model variables.

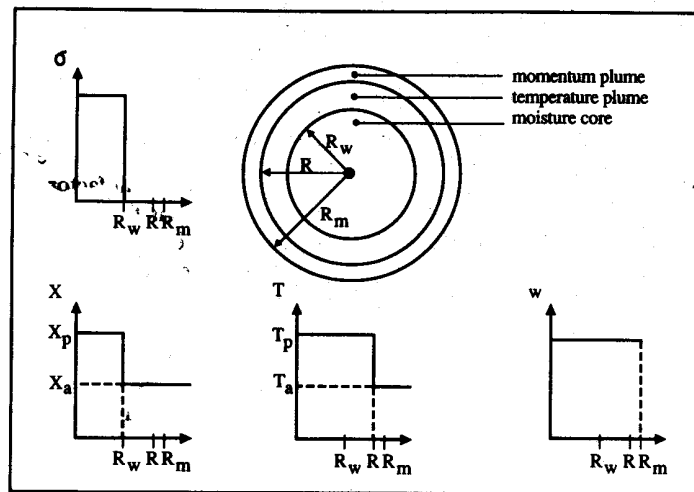


Fig. 2. Three radii of the ANL/UI model: momentum plume, temperature plume and moisture core.

region at the core provides the buoyancy for accelerating the larger momentum-containing region. As a result, buoyancy effects are lessened, which, in turn, contribute to more accurate trajectory/dilution results.

A second problem existing models have in predicting observed plumes is in representing the proper feedback of thermodynamics to plume dynamics due to condensation and evaporation of liquid water. The main physical effect involved is that, as a saturated plume rises, it cools, not at the dry adiabatic lapse rate of  $0.01^{\circ}\text{C m}^{-1}$  but at the saturation adiabatic lapse rate, ranging from  $0.003$  to  $0.007^{\circ}\text{C m}^{-1}$ . Therefore, even when the ambient stratification tends toward stable, the plume can still behave unstably. Under most atmospheric conditions, the inclusion or exclusion of thermodynamics has little effect on the plume predictions of the model. However, in the 10–20% of field cases in which thermodynamics are important, both plume trajectory and plume length predictions are sensitive to thermodynamic assumptions. For example, our findings indicate that in 10–20% of the cases, the models will not be able to predict the very large plumes if the models exclude moisture thermodynamics by treating the sum of liquid and vapor as a passive conserved tracer. Conversely, models will overestimate thermodynamic effects if the models include moisture thermodynamics and assume that liquid water occurs across the entire plume cross-section.

The ANL/UI model is based on experimental data by Hanna (1975), which paves the way for developing a proper assumption for determining the correct thermodynamic feedback on plume dynamics. That assumption is that full thermodynamics will occur, but only across a 'moisture core' at the center of the temperature plume (see Fig. 2, which also illustrates

this assumption). In the ANL/UI model, the ratio of the area of the moisture core to the temperature-elevated core is held fixed (after the zone of flow establishment) at about 50%, a ratio that is in agreement with Hanna (1975). In particular, Hanna observed that a collection of separated parcels or 'clumps' of saturated air with liquid water occupied on average 50% of the plume's cross-sectional area. However, a model with actual parcels need not be adopted, because the same thermodynamic effects are produced if we assume, instead, a continuous moisture core at the center of the plume. Clearly, this assumption leads to thermodynamic effects of intermediate strength that much more accurately represent the observed plume development.

The ANL/UI model also incorporates a separate entrainment formalism during the atmospheric diffusion phase and a physically reasonable additional mixing occurring in the tower wake, thus addressing problem areas 3 and 4 identified in the Introduction above.

### 3. FORMULATION OF THE ANL/UI MODEL

The ANL/UI model is a one-dimensional model, in which the independent variable is taken to be the distance  $s$  along the centerline from the tower outlet plane. The plume is assumed to be axisymmetric for rotations around the centerline in a given cross-section. Variables that describe basic plume geometry are defined in Fig. 1 and in the Nomenclature above. Plume variables such as velocity, temperature, and moisture are assumed to be constant from the centerline out to a corresponding radius. The ANL/UI model contains three separate radii, as described above and as illustrated in Fig. 2. Plume velocity is present from the center out to radius  $R_m$ . The temper-

ature of the plume is elevated from the center out to radius  $R \equiv R_m/\sqrt{v}$ , where  $v$  is a constant to be determined by calibration of the model to field and laboratory data, as discussed below. Plume moisture, and liquid water if present, occupy the region from the center out to a radius  $R_w \equiv \sqrt{\lambda}R = \sqrt{\lambda/v}R_m$ . The constant  $\lambda$  is also to be determined by model calibration. The significance of  $\lambda$  and  $v$  is discussed below.

A set of eight coupled, non-linear, ordinary differential equations for time-averaged steady-state fluxes as a function of  $s$  are solved from initial conditions. The conserved fluxes are mass, horizontal momentum, vertical momentum, enthalpy and total water. There is also an equation insuring that the r.h. of the plume will be 100% whenever liquid water is present. The two geometrical equations that relate  $dx/ds$  and  $dz/ds$  to the plume velocity components complete the set of eight equations as shown in Table 1.

The derivations of the equations are based on mixing a mass  $\Delta m$  of ambient air with a slice of plume air of thickness  $\Delta s$ , while conserving the fluxes and maintaining the saturation condition. The derivations from the conservation laws are lengthy, and since they have been presented in full detail in Carhart *et al.* (1981), they will not be repeated here. The amount of ambient air,  $\Delta m$ , that mixes is parameterized in terms of an 'entrainment velocity'. Let  $\Phi_m$  denote the mass flux for flow through a plume cross-section, as given in Equation (1)

$$\text{mass flux: } \Phi_m = \pi R_m^2 \bar{\rho}_p V. \quad (1)$$

Then the fractional entrainment rate  $\mu$  and the entrainment velocity  $V_e$  are defined by the following:

$$\frac{d\Phi_m}{ds} = \mu \Phi_m, \quad (2)$$

where

$$\mu = \frac{2 \rho_a V_e}{R \bar{\rho}_p V}. \quad (3)$$

It is assumed that the mass  $\Delta m$  of ambient air brings with it centerline ambient values of momentum, heat, and moisture. The four fluxes, in addition to the mass flux, that must be conserved on physical grounds are the following:

$$\text{horizontal momentum flux: } \Phi_{hm} = V_x \Phi_m \quad (4)$$

$$\text{vertical momentum flux: } \Phi_{vm} = W \Phi_m \quad (5)$$

$$\text{enthalpy flux: } \Phi_e = \frac{C_p T_p + \lambda L_v X_p}{v} \Phi_m \quad (6)$$

$$\text{total water flux: } \Phi_w = \frac{X_p + \sigma}{v} \lambda \Phi_m. \quad (7)$$

Separately, the liquid water and the water vapor fluxes are not necessarily conserved. However, their sum, the total water flux, is conserved. The liquid water flux is

$$\text{liquid water flux: } \Phi_{lw} = \frac{\lambda \sigma}{v} \Phi_m. \quad (8)$$

The equation for the flux of liquid water is based on the mixing due to entrainment of ambient air and the assumption that when liquid water is present, the plume relative humidity is exactly 100%. The model differential equations that result from these conservation laws and the specific entrainment assumption used are Equations (9)–(16), as given in Table 1. Where the error is small, the variation of ambient properties with height has been omitted in obtaining these equations. Primitive plume variables of velocity,

Table 1. Governing differential equations for the ANL/UI plume model beyond the region of wake influence and before the atmospheric diffusion phase (see Nomenclature)

$$\frac{d\Phi_m}{ds} = \mu \Phi_m, \quad V_e = \alpha |V - U \cos \theta| + \beta U \sin \theta \quad (9)$$

$$\frac{d\Phi_{hm}}{ds} = (\mu \Phi_m) U; \quad V_x = U \text{ (bentover plume assumption)} \quad (10)$$

$$\frac{d\Phi_{vm}}{ds} = \Phi_m \frac{g}{vV} \left( \frac{T_p^* - T_a^*}{T_a^*} - \lambda \sigma \right) \quad (11)$$

$$\frac{d\Phi_e}{ds} = -C_p \frac{W}{vV} \Phi_m \gamma_d \frac{\rho_a}{\rho_p} + \frac{\mu}{v} \left( C_p T_a + \lambda L_v X_a \right) \Phi_m \quad (12)$$

$$\frac{d\Phi_{lw}}{ds} = \mu \Phi_m \frac{\lambda}{v} X_a \quad (13)$$

$$\frac{d\Phi_{lw}}{ds} = \frac{C_p \Phi_m \chi}{L_v v (1 + \chi)} \left\{ \left( \gamma_d \frac{\rho_a}{\rho_p} + \frac{\Pi}{\tau} \right) \frac{W}{V} + \mu \left[ (T_p - T_a) - \frac{X_p - X_a}{\tau} \right] \right\} \quad (14)$$

$$\frac{dx}{ds} = \frac{U}{V} \quad (15)$$

$$\frac{dz}{ds} = \frac{W}{V} \quad (16)$$

temperature, water vapor, and liquid water may be obtained from the fluxes by solving Equations (1) and (4)–(8) above.

Included within the framework of the model's basic equations in Table 1 are some special features that represent, as accurately as possible, other aspects of the plume's physical behavior. Since details are available in Carhart *et al.* (1981), only a brief description of each feature will be given here.

### 3.1. Plume temperature

As described above, the model assumes different temperature and momentum radii. Studies of air jets with exit densimetric Froude numbers in the range of 0.5–1.0 (typical of NDCTs) show that the temperature-elevated plume area is smaller by a factor of 1.1–2.2 than the momentum-elevated plume area. (See George *et al.*, 1976; Briggs, 1975; Nakagome and Hishida, 1977.) The smaller values have been attributed to plumes without crossflow,<sup>1</sup> while the larger values, according to Briggs, are for highly bentover plumes. The temperature, approximately a passive scalar, mixes radially more slowly than does the momentum. This phenomenon has also been seen in concentration studies.

### 3.2. Plume moisture

As previously, the model assumes a smaller moisture radius than temperature radius. Hanna experimentally showed that the ratio of plume cross-sectional area occupied by saturated clumps or parcels of air was 50% of the total temperature-elevated area. Whether the clumps are contiguous in a 'core' picture, or distributed throughout the plume cross-section, the energetics and the mixing are the same. What does affect the strength of moisture effects is the fractional entrainment rate, and the percentage of plume cross-sectional area occupied by liquid water.

### 3.3. Bentover plume assumption

As introduced above, one of the more successful theoretical assumptions—the 'bentover plume' assumption—has been included in the ANL/UI model. This assumption means that the plume horizontal velocity is taken to equal the ambient velocity at plume height at all times, including immediately on exit from the tower. In one sense, this is like assuming an infinite horizontal drag force whenever the plume's horizontal velocity differs from the ambient velocity. In this model, no vertical drag force is assumed. Davidson (1989) has argued that the 'effective mass' or 'added mass' introduced by using a larger momentum radius than temperature radius is similar in physical effect to a vertical drag force.

### 3.4. Zone for flow establishment

At the tower exit, the three radii— $R_m$ ,  $R$  and  $R_w$ —are all equal, and the profiles are 'top hat' or constant across the exit plane. While the flow is being fully

established as it travels downwind, the profiles change into a Gaussian shape with different widths (represented by equivalent top-hat distributions with different radii). The formula for the length of this zone, as a function of the ratio of the cross-flow velocity to the exit velocity ( $k$ ) is taken from Fan (1967); and the model includes a smooth transition from exit plane conditions to fully established flow conditions that satisfies all conservation equations.

### 3.5. Initial liquid water content

Under conditions that favor large plumes, the amount of initial liquid water assumed for the plume can affect plume length and rise predictions greatly. Consequently, the ANL/UI model incorporates the results of work by Dibelius and Ederhof (1977), which relate readily available tower performance temperatures and ambient conditions to emitted liquid water density,  $\sigma_0$ . In all calibration and verification runs, we used either measured values of  $\sigma_0$ , values computed from the formula of Dibelius and Ederhof, or (if the required temperatures were not reported) a generic liquid water value that is typical of average field measurements, 0.0005 g (liquid water)/g (moist air).

### 3.6. Tower wake effects on trajectory

The low pressure on the downwind side of the tower housing will produce a force at an angle on the plume that is proportional to the square of the wind speed at tower top. The wake can be divided into two major regions: the recirculation cavity and the far wake. The recirculation cavity is the region where mean flow returns toward the body at the center of the wake. The cavity extends several characteristic lengths of the object downwind. The far wake starts at the downwind end of the recirculation cavity, and continues with decreasing measurable effect far downwind. A pressure force is assumed to act on the plume perpendicular to the centerline. This force acts only in the vicinity of the recirculation cavity. Under the bentover plume assumption, the horizontal component of this force has no additional effect. The vertical component of this drag force is

$$F_{wz} = -C_{wf} \rho_p U_0^2 (\sin \theta) \exp[-(x/C_L)^2 - (y/C_w)^2 - (z/C_H)^2]. \quad (17)$$

The  $y$ -dependence in this equation is needed in order to average the wake turbulence over the circumference of the plume cross-section. Formulas for the values of the cavity size factors,  $C_L$ ,  $C_w$  and  $C_H$ , are given in Table 2 for NDCTs and linear mechanical draft cooling towers (LMDCTs). Formulas for other wake parameters, including the offset of the cavity origin from the center of the housing,  $\Delta x_p$ , are also given there. These formulas have been obtained from Lemberg (1973) and Hosker (1979). As discussed below, the single drag force coefficient in Equation (17),  $C_{wf}$ , is fixed during the model calibration phase.

3.7. Tower wake effects on dilution rate

Both the recirculation cavity and the far wake contain enhanced turbulence levels that will cause more rapid turbulent mixing for the plume, if the plume is interacting with the cavity and wake. An additional entrainment velocity was introduced for portions of the plume that interact with either the near or the far wake. The method is adapted from one employed by Halitsky (1977) for dispersion in the vicinity of a nuclear power plant and its associated building complex. An 'effective flat plate' is specified with dimensions related to the dimensions of the building or tower housing. The formulas used for a NDCT and a LMDCT are given in Table 2. Figure 3 shows how we have positioned the effective plates with respect to the shells of the towers. Some interpretation has been necessary to apply data for cylin-

ders and block buildings to the case of cooling tower housings with arbitrary wind directions. For example, the effective plate in Fig. 3 for the NDCT is located at the turbulent boundary layer flow-separation points for a cylinder the diameter of the tower exit, while the plate for the LMDCT has been attached to the up-wind corner of the housing. A standard height of 3 m for external fan shrouds on the LMDCT has also been assumed.

Having established the location and size of the effective plate, Halitsky then uses laboratory data to define empirical fits for the rms turbulence velocity behind such plates from experiments. Assuming no background turbulence (we also have omitted entrainment from background turbulence in our model), the longitudinal rms turbulence velocity behind the structure is estimated from the laboratory

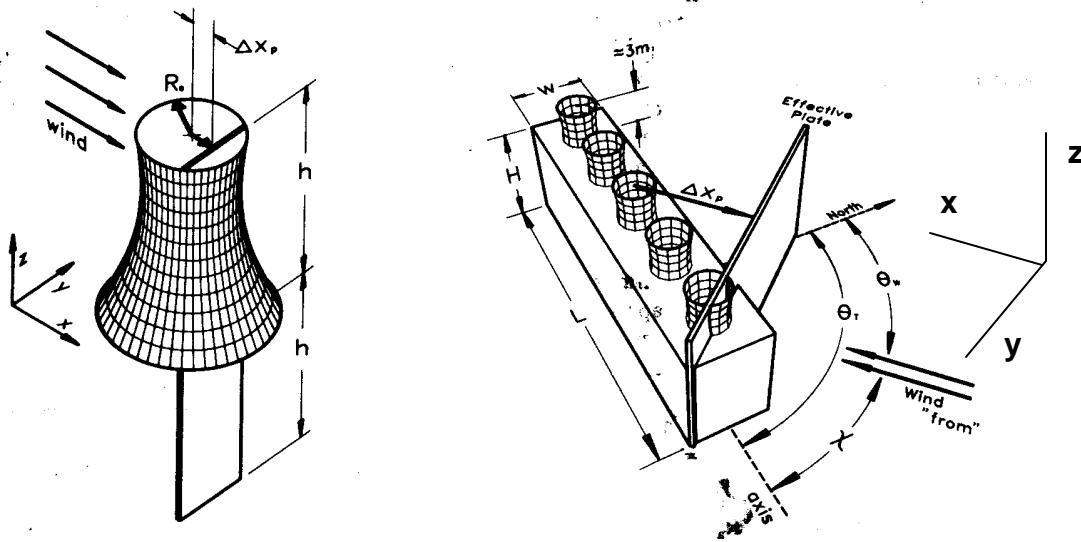


Fig. 3. Plate placement for: (a) NDCT tower housing, and (b) LMDCT tower housing.

Table 2. Formulas for wake parameters introduced in Equations (17)–(20) for NDCTs and LMDCTs with arbitrary wind angle (see Nomenclature and section 3.6)

Parameter	NDCT	LMDCT <sub>c</sub>
$C_H$	$0.5 R_0$	$3 + (1.6)H \cdot \exp[-(1.3)P_L/H]$
$C_L$	$2.0 h$	$X_{CF}(1 -  \cos \psi ) + X_{IL} \sin \psi $
$C_w$	$1.2 R_0$	$(0.55)P_w + (0.85)P_w \cdot \exp[-(0.55)P_w/H]$
$R_a$	$0.866 (R_0/h)$	$P_w/(2H)$
$l$	$1.861 (hR_0)^{1/2}$	$(2HP_w)^{1/2}$
$\Delta x_p$	$-0.5 R_0$	$(0.5) L \cos \psi  - W \sin \psi $

$\theta_r$  = the angle (E of N) made by the tower's long axis (Fig. 3).

$\theta_w$  = the angle (E of N) from which the wind blows.

$\psi = \theta_r - \theta_w$ , the angle between the tower's long axis and the wind.

$X_{IL} = L + (1.75)W/[1 + (0.25)W/H]$ .

$P_H = (H/W)^{1/3}$ .

$P_L = L|\cos \psi| + W|\sin \psi|$ .

$P_w = L|\sin \psi| + W|\cos \psi|$ .

$X_{CF} = W + L[(3.7)P_H - 2]/\{1 + L[(0.305)P_H - 0.15]/H\}$ .

data on flat plates to be

$$\sigma_u = 0.25(x/\ell)^{-2/3}(R_a)^{1/5}\Delta(y, z)U_0, \quad (18)$$

where  $U_0$  is the wind speed at plate top and  $R_a$  is the plate aspect ratio defined as follows:

$$R_a = P_w/(2P_H), \quad (19)$$

where  $P_w$  is the plate width transverse to the wind (horizontal), and  $2P_H$  is the plate height transverse to the wind (vertical). The constant  $\ell$  is the plate characteristic length, which is the square root of the plate's area:

$$\ell = 2P_H R_a^{1/2} = (2P_w P_H)^{1/2}. \quad (20)$$

Again, the  $y$ -dependence is needed to average the turbulent entrainment and drag force over the circumference of the plume cross-section. Halitsky used data from laboratory experiments which employ a flat plate in a cross wind with no ground or other boundary interferences. Therefore, he schematizes his building or other structure of actual height ( $H$ ) with a plate of height ( $2H$ ) in order properly to apply the laboratory data and to cancel the effect of the presence of the ground in the prototype. The far wake, beyond the recirculation cavity, is assumed to be axisymmetric. Its edge or lateral limit,  $r_b$ , is also taken as a semi-circle. The far wake edge grows as  $x^{1/3}$ , while the turbulence intensity from Equation (18) decays as  $x^{-2/3}$ . The turbulence pattern in the recirculation cavity is also assumed to be axisymmetric, although the geometry of the plate makes this approximation less accurate in the cavity. The turbulence levels at any  $x$  in the cavity are equal to those at the end of the cavity.

The distribution in the lateral plane is assumed to be axially symmetric,  $\Delta(y, z) = \Delta(r)$ , where  $r = (y^2 + z^2)^{1/2}$ . The wake boundary,  $r_b$ , is defined as

$$r_b = 1.80(x/\ell)^{1/3}R_a^{-1/10}\ell. \quad (21)$$

It is only through the size of the wake boundary,  $r_b$ , that the  $x$ -dependence enters, and the  $(y, z)$ -dependence enters only in  $r$ . The form of  $\Delta(r)$  that fits laboratory data on plates is

$$\Delta(r) = \begin{cases} 1.167 + 0.167\sin[7.121(r/r_b - 0.221)], & (0 \leq r/r_b \leq 0.441) \\ 0.733 + 0.600\sin[\pi - 5.622(r/r_b - 0.162)], & (0.441 \leq r/r_b \leq 1). \end{cases} \quad (22)$$

To obtain the wake dilution effects in the model, an excess entrainment velocity is then defined by

$$V'_e = C_{wv}\bar{\sigma}_u, \quad (23)$$

where  $\bar{\sigma}_u$  is the rms turbulence velocity as calculated from Equation (18) averaged over the circumference of the plume. The constant  $C_{wv}$  therefore becomes an additional calibration coefficient.

To extend Halitsky's method to include the effects of the recirculation cavity, we assume that the cavity length,  $X_C$ , is related to the plate dimensions by

$$X_C = C_\ell \ell, \quad (24)$$

where  $\ell$  is the plate characteristic length from Equation (20). The constant  $C_\ell$  is a model calibration coefficient. Our calibration of  $C_\ell$  yielded a value of 1.0, whereas the value for actual plates lies between 2 and 3.

### 3.8. Atmospheric diffusion phase

When the rising plume encounters stable ambient air, it eventually reaches zero buoyancy. However, because it still possesses momentum at this point, it keeps rising until it becomes negatively buoyant and then finally stops rising. After this point, the plume air descends and performs a series of oscillations about the zero-buoyancy point that damp out within a few cycles due to continuing entrainment, the Brunt-Vaisala oscillations. The integral plume models are not well formulated to represent the oscillating phase accurately. Therefore, in the ANL/UI model a simplified picture of the leveling-off of the plume in stable air is adopted. When the plume's buoyancy first vanishes, the vertical velocity is set to zero, and the plume variables are readjusted to conserve fluxes. This procedure defines the final height of rise, provided the plume is still visible.

After final rise has been achieved, the plume is considered to be in the atmospheric diffusion phase. Unfortunately, because atmospheric turbulence in elevated inversions is not well studied, only qualitative information is known for plumes in the leveled-off phase. It takes stably stratified air, usually that in the first elevated inversion, to stop the rising plume. In fluid with a strong stable stratification and grid-generated turbulence, it has been shown that eddies that mix vertically die out, while those that mix horizontally do not (Britter *et al.*, 1983). In the atmosphere, this effect seems to give rise to the 'fanning' plumes so often observed in the field—plumes that grow laterally, but not vertically, even over many kilometers (e.g. Davies, 1959). Even the proper time or distance dependence of plume width growth in the horizontal has not been characterized experimentally,

though theoretical estimates of growth as  $x^{2/3}$  and  $x^{2/5}$  have been advanced. Furthermore, it has not been discovered yet how to relate the coefficient of such growth to readily observable meteorological variables.

In light of these uncertainties, therefore, the ANL/UI model does not include a complex atmospheric diffusion submodel, but simply uses an old suggestion of Briggs (1969), obtained from measurements of releases of tracer under neutral conditions. The effective growth rate of these spherical regions of

tracer was measured to be  $x^{3/2}$ . The entrainment velocity implied by these diffusion rates, called  $V_e''$  and given by Equation (25), replaces  $V_e$  in Equation (9) after the zero-buoyancy point is reached, as expressed in the following formula:

$$V_e'' = C_B(UR_m/\bar{z})^{1/3}, \quad (25)$$

where  $\bar{z} = \min\{z+h, 305\}$  in meters,  $h$  is the tower height ( $H+3$  for LMDCTs), and  $U$  is the prevailing wind speed at plume centerline height. The coefficient  $C_B$  is not dimensionless. Due to limited available calibration data for the diffusion phase, no attempt was made to vary  $C_B$  based on atmospheric conditions. Because the plume radius has usually grown very large by the onset of the diffusion phase, properties of the entrained air are taken as average values around the plume periphery of the known  $z$ -dependent ambient properties.

### 3.9. Equivalent flux Gaussian profiles to find visible radius

In determining the size of the visible portion of the plume, equivalent Gaussian profiles for temperature and mixing ratio were used, based on the following equations:

$$T_p(r) = T_a + 2(\bar{T}_p - T_a) \exp(-r^2/b^2), \quad (26)$$

and

$$X_p(r) = X_a + 2(\bar{X}_p - X_a) \exp[-r^2/b^2], \quad (27)$$

where  $b = R/\sqrt{2}$ . The total heat and total water obtained by integrating  $T_p(r)$  and  $X_p(r)$  across a plume cross-section would be the same as taking the constant values  $\bar{T}_p$  and  $\bar{X}_p$  from the center out to the temperature radius  $R$ . Then, the condition for visibility of the plume at radius  $r$  is

$$X_p(r) > Q_s [T_p(r), p]. \quad (28)$$

In this Gaussian assumption, even when the average mixing ratio is subsaturated at the average plume temperature,  $\bar{X}_p < Q_s(\bar{T}_p, p)$ , the centerline mixing ratio can be supersaturated at the central plume temperature  $X_p(0) > Q_s [T_p(0), p]$ .

### 3.10. Freezing of water and thawing of ice

Physically, the liquid water in the plume will usually not freeze as soon as the plume temperature drops below  $0^\circ\text{C}$ . Before spontaneous nucleation and freezing can occur in a cloud water drop, some degree of supercooling is normally necessary, except in the presence of unusually high numbers of condensation nuclei of the proper surface chemistry. Several studies seem to indicate that supercooling by  $10^\circ\text{C}$  typically allows spontaneous nucleation to occur in the natural atmosphere. Therefore, in the ANL/UI model, the liquid water flux in the plume is allowed to freeze instantaneously when the plume temperature reaches  $-10^\circ\text{C}$ . The plume variables  $X_p$ ,  $T_p$ , and  $\sigma$  are then adjusted iteratively to satisfy conservation of total water and conservation of the heat energy of fusion.

Subsequently, the saturation mixing ratio is taken over ice, rather than over water. If the plume happens to heat up again, due to rising through an inversion, the process is reversed, and the ice is melted again to liquid water.

## 4. CALIBRATION OF THE MODEL

### 4.1. Available data

The formulation of the ANL/UI model defines eight adjustable constants that cannot be determined directly from relevant experiments or from theory alone. They must be determined by fitting or calibrating the model to field data and/or to laboratory data on cooling tower plume trajectories and visible plume extent (or measured dilution ratios). These eight constants, with the values subsequently assigned to them, are as follows:

$\lambda$	(0.51) —	determines entrainment when cross-flow is zero
$v$	(1.2) —	determines entrainment rate in diffusion phase
$\alpha$	(0.125) —	determines additional vertical drag force from wake
$\beta$	(0.575) —	determines additional entrainment from wake
$C_B$	(0.34) —	determines length of recirculation cavity.
$C_{wf}$	(0.1) —	
$C_{wv}$	(0.8) —	
$C_L$	(1.0) —	

The data available to us are listed in Table 3, along with the appropriate references. As shown in that table, the data were separated into two portions: the first was used in calibrating the model's coefficients; the second reserved for model verification.

The field data were extensive enough to test all parts of the ANL/UI model's formulation, including moisture thermodynamics, diffusion phase, and visibility criteria. The single-source NDCT data come from three sites in the U.S. and F.R.G., The site in Lünen, F.R.G., had one tower associated with a 335-MWe fossil unit. A larger amount of heat was released at Chalk Point, MD, where the single tower serviced a 600-MWe fossil unit. At Paradise, KY, the single tower cooled an 1100-MWe fossil unit, representing the largest heat release in this study.

On the other hand, the laboratory data permitted the testing of only the basic dynamical formulation of the model, including pressure and wake forces and the entrainment assumption. The data exercise neither the diffusion phase formulation nor the effects of moisture

Table 3. Summary of data used in model calibration and verification

No of towers (cells)	Type	Field or lab	Site or laboratory	No. of cases	References
<i>Calibration</i>					
1	NDCT	Field	Lünen	12	Bremer <i>et al.</i> , 1973
1	NDCT	Field	Chalk Point	14	Meyer, 1975; Meyer and Jenkins, 1977
1	NDCT	Field	Paradise	13	Slawson and Coleman, 1978
1	NDCT	Lab	EDF	6	Viollet, 1977
2	NDCT	Lab	EDF	3	Viollet, 1977
4	NDCT	Lab	EDF	8	Viollet, 1977
1 (6)	LMDCT	Lab	Kannberg/Onishi	6	Kannberg and Onishi, 1978
<i>Verification</i>					
1	NDCT	Field	Chalk Point	2	Meyer and Stanbro, 1977
1	NDCT	Field	Gardanne	5	Viollet, 1977
1	NDCT	Field	Philippsburg	13	Brog and Bhargava, 1984
1	NDCT	Lab	EDF	15	Viollet, 1977
1	NDCT	Lab	Pryputniewicz	3	Pryputniewicz and Bowley, 1975
1	NDCT	Lab	Davis <i>et al.</i>	3	Davis <i>et al.</i> , 1977

thermodynamics. Nevertheless, the laboratory data are very useful, along with the field data, in calibrating the pressure force, wake, and mixing coefficients. Laboratory data were taken in a large water flume at Electricité de France (EDF). The models of one, two, and four NDCTs were designed to produce realistic tower wake effects. Each tower had a scale model housing, and water was withdrawn at the tower base at a rate equal to the heated water emitted. The single-NDCT data with Froude number (defined in the Nomenclature)  $F_0 = 0.65$  were used for calibration. If  $k = (\text{wind speed})/(\text{exit velocity})$ , then data having  $k$ -values in the range of 0.5–3.0 were available, and cases with  $k > 1.5$  showed considerable tower wake effects.

As can be seen from Table 3, the single-source version of the ANL/UI model was calibrated using a mixture of single-source and multiple-source data. Some multiple-NDCT and some single-linear mechanical-draft cooling tower (LMDCT) laboratory data were also used. (The multiple-source extensions of the model are fully described in Part II of this work.) If, as we believe, the basic physics of plume dispersion and wake effects are correctly included in the model, then a single calibration for both single- and multiple-source versions should be possible. Our actual experience in calibration showed that we had to accept some degradation of predictive accuracy for each set of data (single source and multiple sources) in order to achieve a single optimal calibration for both sets of data together. Separate calibrations would have limited the generality and extendability of our model, but would have produced somewhat better performances statistics for the two data sets.

For the NDCT data cases with two towers, the available  $k$ -values were 1, 2, and 3; while for the

NDCT data cases with four towers, the  $k$ -values were 0.5, 1, 2, and 3. The cases of multiple towers with  $k > 1.0$  showed significant tower wake effects. The Kannberg-Onishi data were very similar, except the scale models were of linear mechanical-draft cooling towers. In their single-LMDCT data sets, the available  $k$ -values were 0.6, 1 and 1.5. The latter two  $k$ -values yielded cases with clear tower wake effects.

#### 4.2. Calibration methodology

It seemed unwise to combine all of the available data and to fit the full set of eight coefficients at once, because the solution obtained could easily involve non-physical choices of parameters. When as many as eight parameters are varied simultaneously, there are usually local minima that are not absolute minima on the goodness-of-fit surface. Therefore, our strategy instead was to divide the data in categories from cases containing the least complex physics to those containing the most complex physics. The eight coefficients were then fitted in three successive stages as described below.

4.2.1 *Calibration of entrainment and radii.* The two coefficients  $\alpha$  and  $\beta$  in the entrainment function and the radii coefficients  $\lambda$  and  $\nu$  were determined from only those visible plume data sets of our 39 data cases in which entrainment produced by the plume's own motion through the ambient appeared to dominate throughout plume dispersion. This subset of data cases were required to have  $k$ -values less than 1.2 to minimize wake entrainment; and to possess a visible plume that disappeared during the rising phase, before atmospheric diffusion became dominant. Of the 39 data cases, 13 met these criteria; of these 13 only 10 were employed, because three gave evidence of prob-

lems with the experimental data. The EDF Series A laboratory data with  $k < 1.5$  were also monitored in this phase of calibration. From this point onward,  $\alpha$ ,  $\beta$ ,  $\lambda$  and  $\nu$  were not varied.

4.2.2. *Calibration of atmospheric diffusion.* Those cases to define  $C_B$  were selected from among the 39 visible plume data cases where plumes were long and had leveled off. Only cases where the  $k$ -value was less than 1.2 were selected in order to avoid having the early effects of wake dilution distort the fitting of the atmospheric diffusion phase coefficient. There were five such cases among the 39 visible plume data cases. Optimal statistics were obtained when the value  $C_B = 0.34 \text{ (m/s)}^{2/3}$  was used. This value is close to the value of 0.30 obtained by Briggs (1969), who originated these assumptions for entrainment resulting from ambient turbulence in the free neutral atmosphere. With only five cases to fit this coefficient, we could not easily discriminate both a fitting coefficient and an optimal power law coefficient for the growth of plume width. Given presently available plume data, we do not believe the model would be improved noticeably by using a more realistic picture of a fanning plume.

4.2.3. *Calibration of tower wake effects.* The remaining 16 visible plume data cases had  $k$ -values above 1.2 and showed significant tower wake effects. These were used in determining the three coefficients  $C_{wv}$ ,  $C_{wf}$  and  $C_f$ . Augmenting the visible plume data cases were the selected laboratory data cases. The wake coefficients were determined by fitting results on trajectory and dilution of both the ANL/UI single-source model and the ANL/UI multiple-source model (described in Part II) to the respective laboratory data. The inclusion of both multiple NDCT and LMDCT data in the calibration process is conceptually important, because the primary appeal of Halitsky's equivalent plate formulation for plume/tower wake interaction is its easy generalization to multiple obstacle configurations. The dual calibration approach is used to ensure that one set of coefficients will apply to both single- and multiple-tower applications. Compared with the single-source model, the multiple source model does not have any new calibration coefficients. It differs only in containing a set of assumptions for dealing with the merging of plumes and for computing drag and entrainment for plumes that do not have circular cross-sections. Also monitored in this phase of model calibration were the EDF Series A laboratory data with  $k > 1.5$ , the EDF Series D and E laboratory data for two and four NDCTs, and the Kannberg-Onishi single LMDCT laboratory data.

We noted some conflict in the best-fit values of the three wake-related coefficients between the EDF single-source laboratory data and the field data. The Reynolds numbers for the laboratory data were about  $10^4$ , while those for the field data ranged around  $10^7$ – $10^8$ . These  $Re$  values place the laboratory cases below the critical Reynolds number for the transition from a laminar to a turbulent boundary layer for a

cylinder, and the field cases above the critical value. We feel the differences in boundary layers and consequent differences in the wakes themselves explain the conflict. However, in order to benefit from the extensive laboratory data with a variety of tower housings, we could not bias the fits in favor of field cases. Schatzmann and Policastro (1985) in their single-source Gaussian model that was developed somewhat later than the ANL/UI model, undertook to parameterize this difference. They developed different tower wake effect coefficients for field data and for laboratory data. The tradeoff we experienced was partially alleviated in their work, although the overall performance of the Schatzmann–Policastro model was not markedly better than the ANL/UI model.

#### 4.3. Performance of the ANL/UI model for calibration data

In each step of the calibration process that involved the NDCT field data cases, six quantitative measures of model performance accuracy were monitored, because these measures had proven useful in our earlier model validation work, and values were developed for about 17 models, based on the calibration data base of 39 cases. The six measures are defined as follows, the  $\rho_j$  representing the ratio of predicted plume length or rise to observed length or rise:

$$N_2 = \text{the number of cases for which } 0.5 \leq \rho_j \leq 2.0 \quad (29)$$

$$N_{2.5} = \text{the number of cases for which } 0.4 \leq \rho_j \leq 2.5 \text{ (length only)} \quad (30)$$

$$N_5 = \text{the number of cases for which } 0.2 \leq \rho_j \leq 5.0 \quad (31)$$

$$N_F = \text{the number of cases for which the model failed to make a definite prediction} \quad (32)$$

$$\bar{\rho}_j = N^{-1} \sum_{j=1}^N \rho_j \quad (33)$$

$$\log_{10}(\bar{\rho}_{\log}) = N^{-1} \sum_{j=1}^N |\log_{10} \rho_j|. \quad (34)$$

Table 4 indicates the degree of predictive accuracy for field data cases achieved with the ANL/UI model when it is optimally calibrated by the method described above. This table lists the six statistical measures given in Equations (29)–(34) and standard deviations about the means in Equations (33) and (34) for the ANL/UI model and for four other models from the group of models that performed best on the same 39 data cases in our previous study: the Slawson–Wigley model (Slawson and Wigley, 1975), the Winiarski–Frick model (Winiarski and Frick, 1978), the Hanna model (Hanna, 1975) and the Orville model (Orville *et al.*, 1980). These models did not encompass all of those included in the group of best-

Table 4. Predicted/observed performance measures for five of the best-performing models for both plume rise (above tower) and plume length for the 39 calibration cases of field data, arranged by the log-mean values

Model	$N_2$	$N_{2.5}$	$N_5$	$N_F$	$\bar{\rho}_j$	$\sigma_m$	$\bar{\rho}_{\log}$	$\sigma_{\log}$
<i>Rise</i>								
ANL/UI	30		35	0	0.98	0.41	1.44	0.14
Winiarski-Frick	31		37	0	0.83	0.36	1.49	0.13
Hanna	30		38	0	1.27	0.82	1.60	0.16
Orville	23		35	0	1.74	1.20	1.78	0.20
Slawson-Wigley	17		30	0	0.83	0.68	1.89	0.20
<i>Length</i>								
Hanna	21	23	27	11	1.21	0.71	1.57	0.15
Orville	20	23	32	0	1.72	1.22	1.72	0.22
Winiarski-Frick	23	27	33	0	0.79	0.49	1.77	0.15
ANL/UI	23	30	37	0	1.71	0.97	1.85	0.17
Slawson-Wigley	7	11	24	0	0.72	0.77	2.33	0.19

$\sigma_m$  = Standard deviation of the  $\rho_j$ -distribution.

$\sigma_{\log}$  = Standard deviation of the  $|\log_{10}\rho_j|$ -distribution.

performing models for single NDCT cases in our previous study (Carhart *et al.*, 1982), however, they were the only models in that group for which we were able to assemble a full set of model/data comparisons with calibration and verification data. Other models that seemed well formulated physically and that were well-calibrated to single NDCT laboratory and field data were the KUMULUS model (Moore, 1977; Brog and Bhargava, 1984) and Schatzmann-Policastro model.

As we can see from Table 4, the ANL/UI model is among the best-performing models for the field data. It can clearly predict plume rise as well as or better than any other model, and within a factor of 2.0 in 75% of cases. It is very reliable under a wide range of wind speeds, humidities, and lapse rates, and always yielded a definite rise prediction for these data. However, for plume length, the ANL/UI model tends to overpredict more than does the Orville or Winiarski-Frick model. From an environmental impact viewpoint, this tendency is desirable because such predictions are conservative. However, from a physical point of view, such predictions must be considered somewhat more inaccurate. The model is more reliable than any other, as judged from its  $N_5$  and  $N_{2.5}$  values. In fact, we can say that the ANL/UI model is able to predict plume length within a factor of 2.0 in 60% of cases and within a factor of 2.5 in 75% of cases, though with a tendency to overpredict plume length somewhat.

One clear strength of the ANL/UI model is its inclusion of a definite formulation for tower wake effects on the plume, a feature shared only by the KUMULUS model and the Schatzmann-Policastro model. Only the Schatzmann-Policastro model has a more detailed formulation, which also include a dependence on Reynolds number. The value of including such a formulation is clearly evident in Fig. 4, which summarizes the laboratory NDCT data from EDF.

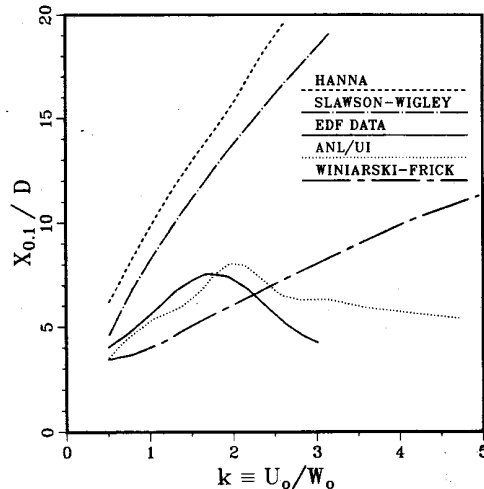


Fig. 4. EDF data and predictions for four best-performing models for downwind distance to tenfold dilution with increasing wind speed (the quantity  $x_{0.1}$  is the downwind distance where centerline concentration excess ratio reaches 0.1 of its initial value,  $\Delta C = 0.1 \Delta C_0$ ).

The  $k$ -value was varied from 0.5 to 3.0 in five steps, and the distance downwind at which a 10:1 dilution occurred on the centerline was measured. Figure 4 shows the data and predictions of four of the same five models presented in Table 4. (We could not obtain Orville model results for these data.) The fact that the distance to 10:1 dilution first increases with  $k$ , and then decreases for  $k$  above about 1.5, is accounted for only by the ANL/UI model.

To quantify model predictive performance for the field data, we have chosen to present absolute-log-mean values as defined in Equation (34). For the laboratory data points, as for the field data, the ratio  $\rho_j$  is defined as the ratio of predicted plume rise or

concentration to the respective observed value. The only difference is that the plume 'rise' is computed with respect to the ground, rather than with respect to the tower top. This is necessary for the laboratory data, otherwise the small rise values near the tower exit would seriously distort the statistics. For the stagnant ambient cases, the vertical velocity values are used instead, because, in a crossflow case, these values are physically most closely related to trajectory. The use of the absolute-log-mean ensures that both underprediction and overprediction of values will contribute to a ratio greater than 1.0. In fact, when these averages were calculated over a large number of predicted/observed pairs, the average fractional error in predictions for all of the models came out close to  $(\bar{\rho}_{10g} - 1)$ .

Table 5 presents the value of  $\bar{\rho}_{10g}$  for all five models. The superiority of the ANL/UI model is evident, and is due mainly to its superior tower wake formulation for  $k > 1.5$ . Figure 5 shows a typical pair of graphs for the most extreme case,  $k = 3$ . Among the models compared, only the ANL/UI model is capable of representing the lowered trajectory due to wake suction, as well as the increased mixing due to wake turbulence. Also included in Table 5 values are statistics for multiple-NDCT and single-LMDCT laboratory data (EDF series D and E and Kannberg-Onishi in crossflow and in-line configurations). We had available results from only two of the other models for the multiple-source data, which were used in the calibration of the ANL/UI model. The ANL/UI model usually produces predictions that are more accurate than those produced by the other models. It is the best-performing model for trajectory and dilution among the models that were run for all single and multiple source laboratory data (Slawson-Wigley and Orville).

The fact that the ANL/UI model performs well with the laboratory data gives us confidence in the physics of its entrainment and wake formulations. All models have been calibrated to some subset of these field and laboratory data cases, and the better-performing models have comparable statistics to the ANL/UI model within statistical errors. If the model does not do well separately for the laboratory data cases as compared to field cases (e.g. the Orville model), then physical effects present in the field cases

due to water vapor may have been calibrated to offset the effects causing only dilution and bending. However, in new cases or cases outside the range of parameters encountered in calibration cases, such models will probably not predict accurately, because separate physical effects are not calibrated properly. The ANL/UI model should continue to show good predictive accuracy in verification tests, because of separate calibration of force and dilution effects (using both laboratory data and field data), and of moisture thermodynamic and atmospheric diffusion effects (using field data).

## 5. VERIFICATION OF THE MODEL

Once calibrated, a model needs to be tested further or verified with new data not utilized in the calibration phase. Good model/data comparisons for verification data give us confidence that the model can predict new cases for which it has not been calibrated, especially if the parameters characterizing the verification data lie outside the range of the parameters of the calibration data. The data reserved to verify the ANL/UI model are outlined in the second section of Table 3.

### 5.1. Verification field data

In the category of field data, two new Chalk Point cases became available after the model was calibrated, along with five cases from a small NDCT at Gardanne, France. At Gardanne, the tower dissipated heat from a 250-MWe fossil-fueled plant, which is somewhat less heat than was dissipated by the smallest tower represented in the calibration data (Lünen). The Gardanne cases contained small saturation deficits, but the humidity measurements were subject to considerable error, reducing the value of data that would otherwise place a stringent test on model performance. The ANL/UI and Orville models were run for these data sets.

Also published after the ANL/UI model was calibrated were 13 cases from a tower dissipating heat from a 1800-MWe fossil-fueled plant at Philippsburg, F.R.G., against which several European and American models were tested. The heat released by this tower is much larger than that released in any of the

Table 5. Laboratory data values of  $\bar{\rho}_{10g}$  for trajectory and dilution predictions of five models for both calibration and verification data cases: number of trajectory cases = 23 calibration, 18 verification; number of dilution cases = 23 calibration, 21 verification

Model	Trajectory			Dilution		
	Cal.	Verif.	Total	Cal.	Verf.	Total
ANL/UI	1.21	1.19	1.20	1.31	1.27	1.29
Winiarski-Frick*	1.45	1.27	1.32	1.41	1.23	1.27
Hanna*	1.44	1.44	1.44	2.36	1.58	1.72
Slawson-Wigley	1.61	1.45	1.54	1.71	2.72	2.24
Orville	2.04	1.45	1.71	3.34	1.60	2.07

\* Based on 17 fewer cases.

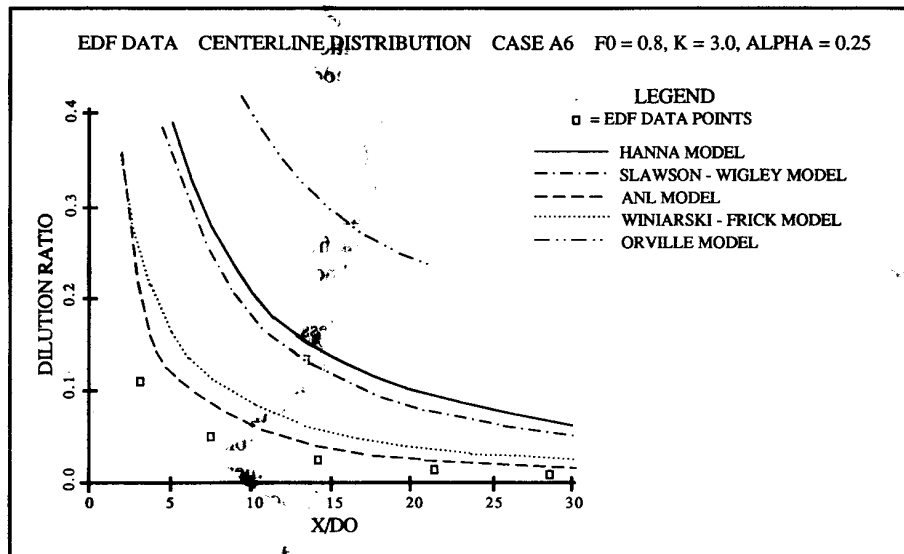
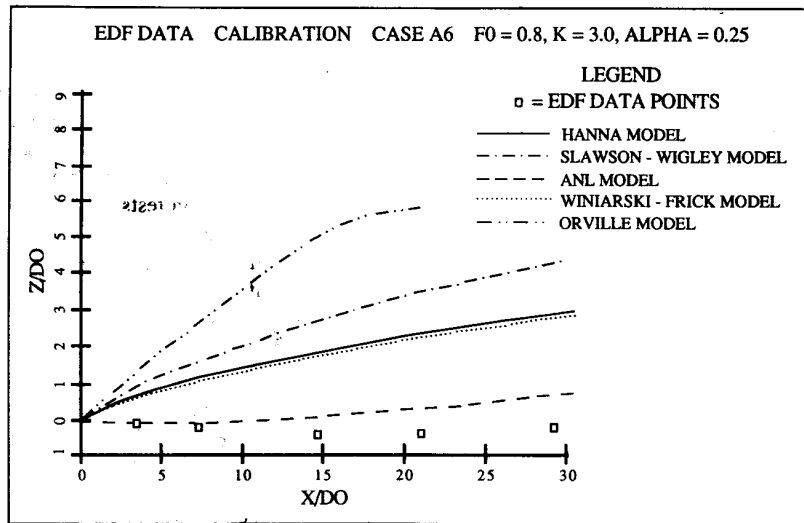


Fig. 5. Comparison of five best-performing models to EDF laboratory data: (top) centerline trajectory; (Bottom) centerline dilution.

calibration cases, and the models are being tested outside the range of parameters for which they were calibrated. Figure 6 shows typical visible plume predictions of the ANL/UI model and the Winiarski-Frick model for Philippsburg, case 9. This case has a moderately long plume under near-neutral ambient conditions. The model performance statistics for the five models compared earlier are given in Table 6 for the combined calibration and verification field data. For the ANL/UI and Orville models, the statistics are presented both with and without the Chalk Point and Gardanne verification data sets. The added difficulty that both models had with the five Gar-

danne and two Chalk Point data cases can be traced primarily to the Gardanne data, where we believe the larger uncertainty in r.h, coupled with small saturation deficits, caused excessive errors in the predictions of both models. We do not recommend the use of these seven data cases in future visible plume model calibrations or studies. Comparison of Table 6 with Table 4 shows that the models had very similar performance statistics on the calibration cases and on the verification cases, within the statistical errors indicated in the tables. This consistency of predictive performance is encouraging. However, for all rise predictions the absolute-log-mean shows moderate

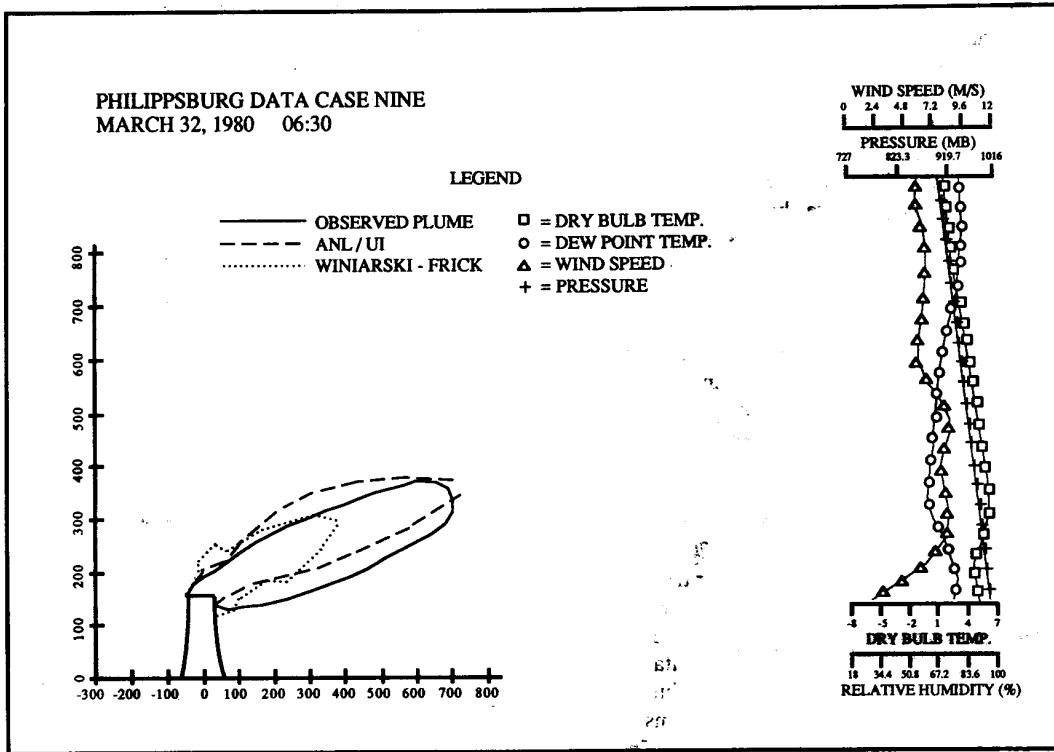


Fig. 6. Philippsburg data case 9: comparison of visible plume with ANL/UI and Winiarski-Frick model predictions.

Table 6. Predicted/observed performance measures for five of the best-performing models for both plume rise (above tower) and plume length arranged by log-mean for the combined data base (39 calibration field cases and 13 verification field cases).

Model	$N_2$	$N_{2.5}$	$N_5$	$N_F$	$\bar{\rho}_j$	$\sigma_{sm}$	$\bar{\rho}_{log}$	$\sigma_{log}$
<i>Rise</i>								
ANL/UI	40		48	0	1.10	0.50	1.45	0.14
	43		55	0	1.02	0.54	1.53	0.16
Winiarski-Frick	40		50	0	0.90	0.52	1.52	0.14
Hanna	36		49	0	1.49	0.94	1.69	0.18
Orville	30		47	0	1.81	1.14	1.81	0.20
	33		53	0	1.79	1.15	1.85	0.19
Slawson-Wigley	27		43	0	0.93	0.77	1.80	0.19
<i>Length</i>								
Hanna	25	28	32	15	1.19	0.71	1.57	0.15
Orville	29	35	44	0	1.63	1.10	1.68	0.20
	31	38	50	0	1.64	1.14	1.74	0.21
Winiarski-Frick	30	38	46	0	0.80	0.50	1.79	0.14
ANL/UI	30	37	46	2	1.74	0.98	1.81	0.18
	33	41	51	2	1.73	1.00	1.81	0.18
Slawson-Wigley	11	16	33	3	0.64	0.66	2.36	0.18

Note: values for ANL/UI and Orville are also given which utilize the additional seven Gardanne and Chalk Point cases, totalling 59 calibration and verification cases.

0.54

degradation when the verification field data are included. For length predictions, all models except the ANL/UI model show loss of accuracy in the absolute-log-mean, while the ANL/UI model exhibits a slight gain in accuracy.

5.2. Verification laboratory data

Only single-tower laboratory data were held in reserve for model verification. (Multiple-tower cases available for verification are discussed in Part II of this work.) The EDF series B data (four cases) with

$F_0=2.0$  had model tower housings with  $H/D=0.55$  and  $k$ -values of 0.3, 0.6, 0.8 and 1.0. These values represent typical dimensionless parameters for a circular MDCT, for which an effective single source is usually expected to yield a good approximation. On the other hand, the series C EDF data with  $F_0=0.4$  clearly represent a NDCT. Series C data exhibit strong effects of the tower wake, because they include  $k$ -values between 3 and 5. This series also includes one pure momentum jet case with  $F_0=50$  and  $k=2.5$ .

Data taken in a stagnant ambient with neutral stratification are very useful in testing the calibration of one of the two entrainment coefficients ( $\alpha$ ) apart from other considerations but as a function of Froude number. Since there is no trajectory, the vertical velocity measurements are used instead; the dilution data are available as they are for the crossflow cases. The nine stagnant ambient cases represent three from EDF, three from Pryputniewicz and Bowley (1975), and three from Davis *et al.* (1977). The three EDF cases had  $F_0=0.55, 1.1$  and  $2.4$ , and for these cases the velocity decay predictions were used in place of the trajectory predictions in the performance statistics. For the three cases of Pryputniewicz data, also in a water flume with heated effluent, only dilution values were presented, and no velocity predictions could be compared. The  $F_0$ -values were 1, 2 and 4. The Davis *et al.* (1977) data were taken with salt water issuing into fresh water to achieve buoyancy. Froude numbers were 1.5, 3 and 6.

The five models compared earlier in their performance for the calibration laboratory data were also run for the verification laboratory data. Again, the value of  $\bar{\rho}_{\log}$  was computed as an overall measure of model predictive accuracy. The values are included in Table 5 for predicted trajectories and dilutions, respectively, as well as the values for the combined calibration and verification data. As shown, the Winiarski-Frick model performs more accurately for the verification data than for the calibration data, especially for the dilution data. For the verification dilution predictions, the Winiarski-Frick model achieves the same predictive accuracy as does the ANL/UI model. This is not surprising, because, in calibrating their model, Winiarski and Frick relied heavily on some of these stagnant ambient cases. Also, the competitive performances of the Winiarski-Frick model and of the Hanna model are difficult to determine from these numbers, because these two models were not formulated to make predictions for the multiple-source laboratory cases. Thus, their statistics exclude a number of cases that other models had difficulty with, and, for the Winiarski-Frick model, included cases to which the model was calibrated.

For the verification data comparisons, the ANL/UI model again showed superior ability to predict the observed trajectories, especially in cases of large  $k$  (large wake effects), and competitive ability to predict dilutions.

## 6. CONCLUSIONS

This paper has presented the theory, calibration, and verification of a new state-of-the-art integral model for predicting cooling tower plume rise and dispersion. The ANL/UI plume dispersion model has been embedded in an integrated set of computer codes that can perform seasonal/annual environmental impact assessment, including visual plume impact, drift deposition, fogging, icing and shadowing (Policastro *et al.*, 1984). The system, called the Seasonal/Annual Cooling Tower Impact Prediction Code (SACTIP), uses readily available data from the U.S. National Climatic Center in Asheville, NC, and allows averaging over extended periods of data, from 1 to 5 yr or more. In that system, frequency-of-occurrence statistics are first computed from the full set of meteorological records, and the statistics are then used to determine a set of about 35 representative categories of plumes and average meteorological conditions for each category. Next, the ANL/UI model described in this paper is used to run detailed predictions for the average meteorological conditions and average exit conditions of each category for up to five significantly different wind directions determined from the actual source configuration. Finally, each set of category-representative detailed case predictions are distributed according to frequency-of-occurrence by wind direction of that category. In this way the superior predictions of an integral model such as the ANL/UI model can be readily used to predict environmental impacts of cooling towers and similar sources.

For field data cases, we have seen that the ANL/UI model is able to predict visible plume rise within a factor of 2.0 in 75% of cases, and visible plume length within a factor of 2.5 in 70% of cases. For laboratory data cases, the absolute-log-mean error in trajectory predictions was 20% of rise above the ground. The absolute-log-mean error in dilution predictions was 30%. Such levels of predictive accuracy can now be considered state-of-the-art for one-dimensional integral models. Several other models can achieve this accuracy of prediction for single-source field and laboratory cases, but none of them has a separate methodology for multiple-source cases. To achieve accurate prediction for multiple sources, a model must have the ability to follow each emerging plume until they have all joined into a single plume. This is especially the case when NDCTs occur in separated clusters, or when MDCTs are long or more than one MDCT housing is present.

If further field or laboratory studies are planned to test and validate cooling-tower plume models, the experiments should develop a number of cases with high  $k$ -values to further test the adequacy of the formulation of tower wake effects in predicting dilution and trajectory. Actual mixing measurements in the wake would be very helpful. Also, a variety of cases with conditional instability in the ambient

should be included with a variety of dimensionless parameters, as well as cases where the visible plume enters the atmospheric diffusion phase and is carefully documented as to extent and length in that phase. Any further developments in the accuracy of the individual parametrizations used in the model should be included as they become available. Eventually the ANL/UI model should be recalibrated and reverified with an expanded data base.

## REFERENCES

- Bremer P. et al. (1973) Bericht über die meteorologische Meserie am Standort Lünen vom 27.11.1972 bis 1.12.1972 Zur Teilüberprüfung und Vereinerung des numerischen Modells SAUNA, Arbeitsgruppe über die meteorologischen Auswirkungen der Kühltürme, Dienst für Luftreinhaltung der Schweizerischen Meteorologischen Zentralanstalt, Payern.
- Briggs G. A. (1969) Plume Rise, AEC Critical Review Series, USAEC Report TID-25075, Nov. 1969.
- Briggs G. A. (1975) Plume rise. In *Proceedings of the Workshop on Meteorological and Environmental Assessment*. American Meteorological Society, Boston, MA.
- Britter R. E., Hunt J. C. R., Marsh G. L. and Snyder W. H. (1983) The effects of stable stratification on turbulent diffusion and the decay of grid turbulence. *J. Fluid Mech.* **127**, 27–44.
- Brog P. and Bhargava B. (1984) Untersuchung des Betriebsverhaltens, der Emission and der Schwadenausbreitung, durchgeführt am Naturzug-Naßkühlturm des Kernkraftwerks Philippsburg, Block 1 (revised by W. Hofmann, May 1982). In *Naturzug-Naßkühlturm des Kernkraftwerkes Philippsburg (Block 1). Ergebnisse der Schwadenausbreitungsrechnungen* (edited by Ernst G.). *Fortschritt-Berichte der VDI Zeits.* Reihe 15, Nr. 30, pp. 164–220.
- Carhart R. A., Policastro A. J. and Ziemer S. (1982) Evaluation of mathematical models for natural-draft cooling tower plume dispersion. *Atmospheric Environment* **16**, 67–83.
- Carhart R. A., Policastro A. J., Ziemer S., Haake K. and Dunn W. (1981) Studies on mathematical models for characterizing plume and drift behavior from cooling towers, Vol. 2. Mathematical model for single-source (single-tower) cooling tower plume dispersion. Electric Power Research Institute Report CS-1683, Vol. 2, Palo Alto, CA.
- Davidson G. A. (1989) Simultaneous trajectory and dilution predictions from a simple integral plume model. *Atmospheric Environment* **23**, 341–349.
- Davies R. W. (1959) Large-scale diffusion from an oil fire. *Adv. Geophys.* **6**, 413–415.
- Davis L. R., Shirazi M. A. and Slegel D. L. (1977) Measurement of buoyant jet entrainment from single and multiple sources. Paper No 77-S-1101 of AIChE-ASME Heat Transfer Conference, Salt Lake City, Utah, 15–17 August.
- Dibelius G. and Ederhof A. (1977) Correlation experiments for recondensed and entrained water in cooling towers. In *Wet Cooling Towers: Thermal Principles and Measurements* (edited by Rögner H.), VDI Report 298, pp. 17–21. VDI-Verlag GmbH. (Proceedings of seminar held in Düsseldorf, 25 May 1977.)
- Fan L. N. (1967) Turbulent buoyant jets into stratified or flowing ambient fluids. W. M. Keck Lab. of Hyd. and Water Res., Report No. KH-R-18, California Institute of Technology, Pasadena, CA.
- George W. K., Alpert R. L. and Tamanini F. (1976) Turbulence measurements in an axisymmetric buoyant plume, Basic Research Dept. Technical Report 22359-2, RC-B-53, Factory Mutual Research, Norwood, MA.
- Halitsky J. (1977) Wake and dispersion models for the EBR-II building complex. *Atmospheric Environment* **11**, 577–596.
- Hanna S. R. (1975a) Predicted and observed cooling tower plume rise and visible plume length at the John E. Amos power plant, ATDL No 75/21. Atmospheric Diffusion Laboratory, Oak Ridge, TN.
- Hanna S. R. (1975b) Predicted and observed cooling tower plume rise and visible plume length at the John E. Amos power plant. *Atmospheric Environment* **10**, 1043–1052.
- Hosker R. P., Jr (1979) Flow and diffusion near obstacles. In *Atmospheric Science and Power Production Chapter 7* (edited by Randerson D.), DOE/TIC-27601, pp. 241–326. NTIS, Springfield, VA.
- Kannberg L. and Onishi Y. (1978) Plumes from one and two cooling towers. In *Environmental Effects of Atmospheric Heat/Moisture Releases. Cooling Towers, Cooling Ponds, and Area Sources* (edited by Torrance K. and Watts R.). ASME, New York, New York. Presented at Second AIAA/ASME Thermophysics and Heat Transfer Conference, Palo Alto, CA, 24–26 May 1978.
- Lemberg R. (1973) On the wakes behind bluff bodies in a turbulent boundary layer. Wind Tunnel Report No. BLWT-3-73, University of Western Ontario, London, Ontario, Canada.
- Meyer J. H. (1975) Chalk Point surface weather and ambient atmospheric profile data, first intensive test period, 15–19 December 1975 (revision). Applied Physics Lab., Johns Hopkins Univ., PPSP-CPCTP-4REV (and Environmental Systems Corporation document PPSP-CPCTP-8).
- Meyer J. H. and Jenkins W. R. (1977) Chalk Point surface weather and ambient atmospheric profile data, second intensive test period, 14–24 June 1976. Applied Physics Lab., Johns Hopkins Univ., PPSP-CPCTP-11 (and Environmental Systems Corporation document PPSP-CPCTP-12).
- Meyer J. H. and Stanbro W. D. (1977) Chalk Point cooling tower project, cooling tower project final report FY 1977, Vols. 1 and 2. Cooling Tower Drift Dye Tracer Experiment, 16 and 17 July 1977. JHU PPSP-CPCTP-16. The Johns Hopkins University, Applied Physics Laboratory, Laurel, MD.
- Moore R. D. (1977) The KUMULUS model for Plume and Drift Deposition Calculations for Indian Point Unit No. 2. Environmental Systems Corporation, Knoxville, TN.
- Nakagome H. and Hishida M. (1977) The structure of turbulent diffusion in an axisymmetric thermal plume. In *Turbulent Buoyant Convection*, pp. 361–372. Proceed. of the International Center for Heat and Mass Trf., Dubrovnik, Yugoslavia.
- Orville H. D., Hirsch J. H. and May L. E. (1980) Application of a cloud model to cooling tower plumes and clouds. *J. appl. Met.* **19**, 1260–1272.
- Policastro A. J. et al. (1984) User's manual: cooling-tower-plume prediction code. Electric Power Research Institute, Report No. EPRI CS-3403-CCM (228 pages). April 1984.
- Pryputniewicz R. J. and Bowley W. W. (1975) An experimental study of vertical buoyant jets discharged into water of finite depth. *Trans. of the ASME J. Heat Trans.* **274**–281.
- Schatzmann M. and Policastro A. J. (1985) An advanced integral model for cooling tower plume dispersion. *Atmospheric Environment* **18**, 663–674.
- Slawson P. R. and Coleman J. H. (1978) Natural-draft cooling-tower plume behavior at Paradise steam plant, Part II. Tennessee Valley Authority, Division of Environmental Planning, TVA/EP-78-01, February 1978.
- Slawson P. and Wigley P. M. (1975) The effects of atmo-

- spheric conditions on the length of visible cooling tower plumes. *Atmospheric Environment* **9**, 437-445.
- Viollet M. P.-L. (1977) Étude de jets dans des courants traversiers et dans des milieux stratifiés. These de Docteur-Ingénieur, Université P. et M. Curie, Paris.
- Winiarski L. and Frick W. (1978) Methods of improving plume models. Cooling Tower Environment—1978. *Proc. Power Plant Siting Commission, Maryland Dept. of Natural Resources*. PPSP-CPCTP-22. WRRRC Special Report No. 9.